Birkeland current system key parameters derived from Iridium observations: Method and initial validation results

B. J. Anderson,[1] K. Takahashi,[1] T. Kamei,[2] C. L. Waters,[3] and B. A. Toth[1]

Received 12 March 2001; revised 16 July 2001; accepted 17 August 2001; published 19 June 2002.

[1] The Iridium satellites in 780 km altitude, circular polar orbits provide continuous global monitoring of the Birkeland current system via engineering magnetometer data. These data have been used to characterize basic features of the global field-aligned currents (FACs) with a time window of 45 min and a time step of 15 min. The three sigma magnetometer data noise threshold is 93 nT on average. The fraction of measurements above the noise is used to provide one measure of the location of the auroral FACs. Measures are also presented for the mean latitude and equatorward/poleward extent of the region 1/region 2 FAC system. The equatorward latitude of region 1/region 2 FACs is anticorrelated with *Kp*, $r = -0.68$. Indices are presented for the net FAC intensity in terms of the eastward (westward) magnetic perturbation in the northern (southern) hemisphere by analogy with the *AE*, *AU*, and *AL* indices. The Iridium system indices show high correlation with the quick look auroral electrojet indices both in individual cases and statistically, $r = +0.73$ between their logarithms. Results are presented for two storms, 22–23 September 1999, *Dst* minimum approximately −160 nT, and 21–22 October 1999, *Dst* minimum approximately −230 nT, reflecting that intensification and equatorward expansion of the global FACs occur in response to southward IMF. Enhanced dynamic pressure promotes more rapid equatorial expansion, 10° in 1.5 hours for the September storm, for which the dynamic pressure was enhanced, 15–20 nPa, at southward IMF turning, as opposed to the October case, 13° over ∼8 hours, for which the southward turning occurred during nominal dynamic pressure, ∼5 nPa. In both storms the current intensity decreases to prestorm levels within an hour when the IMF turns northward or nearly horizontal, at the beginning of storm recovery. The key parameters are a useful means of accessing the Iridium system data for preliminary analyses, and the initial results provide motivation for future analyses to quantify the accuracy and reliability of products derived from the Iridium system data. *INDEX TERMS:* 2708 Magnetospheric Physics: Current systems (2409); 2736 Magnetospheric Physics: Magnetosphere/ionosphere interactions; 2407 Ionosphere: Auroral ionosphere (2704); 2794 Magnetospheric Physics: Instruments and techniques; 2788 Magnetospheric Physics: Storms and substorms; *KEYWORDS:* Iridium constellation, Birkeland field-aligned currents

1. Introduction

[2] Since the signatures of the Birkeland field-aligned currents (FACs) were first detected [*Zmuda et al.*, 1966] and interpreted [*Cummings and Dessler*, 1967], it has been recognized that they couple stresses between the magnetosphere and ionosphere [*Cowley*, 2000]. Measuring their distribution has therefore been a major observational objective [*Armstrong and Zmuda*, 1973; *Iijima et al.*, 1978, 1990; *Iijima*, 2000]. Our present understanding of the Birkeland system is largely based on statistical analyses of low-altitude data sets from individual satellites which use months of data to accumulate a distribution of measurements to infer FAC patterns [*Iijima and Potemra*, 1976a, 1976b; *Weimer*, 2000]. Since the currents depend on the interplanetary magnetic field (IMF) [*Zanetti et al.*, 1983; *Iijima*, 1984; *Erlandson et al.*, 1988; *Watanabe et al.*, 1996], which, in turn, is variable on timescales of minutes to hours, we expect the global FAC distribution to be highly variable as well. Single-pass satellite data, however, do not provide the wide spatial coverage required to obtain information about the instantaneous pattern or dynamics of the currents [e.g., *Ohtani et al.*, 1995; *Weimer*, 2000].

[3] Distributions of FAC have been inferred from ground-based observations. The Kamide-Richmond-Matsushita (KRM) method [*Kamide et al.*, 1981] and the related Assimilative Mapping of Ionospheric Electrodynamics (AMIE) procedure [*Richmond and Kamide*, 1988] use a combination of distributed data and statistical models of ionospheric conductivities to infer the spatial distribution of ionospheric parameters from which the FACs are calculated. The KRM algorithm was developed to use ground magneto-

[1]The Johns Hopkins University Applied Physics Laboratory, Laurel, Maryland, USA.
[2]World Data Center, Kyoto University, Kyoto, Japan.
[3]School of Mathematics and Physical Sciences, University of Newcastle, Callaghan, New South Wales, Australia.

Copyright 2002 by the American Geophysical Union.
0148-0227/02/2001JA000080$09.00

meter data only, and although AMIE principally uses ground magnetometer data, it can use satellite electric field, particle, and magnetic field data when available [e.g., *Lu et al.*, 1996]. The conductivity models, modified using satellite and ground data, are used to infer Hall currents, the electric field, the horizontal currents, and, finally, the FACs. Electric field distributions determined from radars have also been used to infer FACs, but the conversion to Birkeland current also depends on the assumed conductivity distribution [*Sofko et al.*, 1995]. It would be highly desirable to determine FAC distributions without dependence on statistical conductivity models. In addition, during geomagnetic storms the aurora and their current systems can expand equatorward of ground observatories, so that we have limited knowledge of these conditions.

[4] The Iridium satellite constellation provides an opportunity to characterize global-scale Birkeland currents. To date, the most direct detection of FACs is from the magnetic perturbations they generate above the ionosphere. These perturbations are often hundreds of nT below 2000 km altitude and are readily detected from low Earth orbit [e.g., *Armstrong and Zmuda*, 1973]. Each Iridium satellite carries an engineering magnetometer, and techniques have been developed to reduce these data to yield the satellite cross-track magnetic perturbations associated with the Birkeland currents [*Anderson et al.*, 2000]. Beginning 18 February 1999, data that were already being obtained for operations were made available for scientific study. The Iridium system consists of more than 70 satellites in circular, polar, 780 km altitude orbits in six equally spaced planes. The orbit plane spacing provides ~0200 MLT resolution. In contrast to ground systems, there are no major gaps, greater than >2 hours, in local time coverage, and the FACs never expand equatorward of the system. The system also provides continuous time coverage with no time gaps due to diurnal or orbital periods and gives comparable coverage in the northern and southern hemispheres.

[5] Since the satellites and instrumentation were not designed or qualified for this purpose, it is important to verify that the Iridium system provides meaningful data on high-latitude FACs. That the engineering magnetometers have adequate sensitivity and that the data can be processed to extract FAC signatures have been demonstrated previously [*Anderson et al.*, 2000]. *Waters et al.* [2001] developed spherical harmonic fitting (SHF) techniques to derive the global magnetic perturbation maps and FAC patterns from the Iridium data and presented initial validation checks using Defense Meteorological Satellite Program (DMSP) magnetometer and Polar UVI data. The magnetic perturbation map agreed with the DMSP data to within the latitude resolution (~2°) and uncertainty (~100 nT) in the Iridium data, and the upward FACs corresponded to regions of discrete auroral emissions [*Waters et al.*, 2001].

[6] In addition to the SHF technique, it is essential to have a set of quantities that offer an overview of the information content in the Iridium constellation magnetometer data that can guide further analysis. For magnetometer data from a single satellite this usually consists of time series plots of the three components. The Iridium constellation data are not well suited to this approach since a collection of seventy or more time series is too unwieldy to interpret. Moreover, the content of the constellation data is qualitatively different from data obtained by a single satellite; one is interested in the information content of the entire collection of measurements. In order to access the data we found it necessary to develop a new set of key parameter-like products.

[7] Although the SHF technique presented by *Waters et al.* [2001] is a powerful tool for detailed analysis, it is inappropriate for providing key-parameter summary information of the Iridium data set. It was developed to derive quantitative estimates of field-aligned current density and vector maps of magnetic perturbations in analyzing specific events in detail. Survey products need to reflect the basic features of the original data as closely as possible. This is particularly important for the Iridium data set since it is from satellites and instruments not designed for scientific research.

[8] There are two other reasons for developing different products as key parameters. The southern hemisphere SHF results are not as robust as those from the northern hemisphere. The geographic pole is usually within the region of field-aligned currents in the southern auroral zone. Because only cross-track data are suitable for analysis, the region near the geographic pole is difficult to fit. The procedure interpolates across a 4° circular region over the geographic pole [cf. *Waters et al.*, 2001]. This approach meets with varied success, and as a result, the SHF technique does not reliably provide comparable measures of the northern and southern hemisphere data.

[9] Evaluating SHFs for all of the data is also logistically more difficult. The SHF procedure requires ~100 times more processing time than the quantities described below and involves additional file transfers and an approximate doubling of file space. The fact that the research is conducted under constrained resources means that these practical matters are not merely issues of convenience.

[10] In this paper we therefore introduce a set of measures derived from the Iridium data that serve as continuous key parameters that provide an invaluable complement to the SHF analysis. These summary data products were developed specifically to access and work with the data, and we have found them to be indispensable for more in-depth analyses. The Iridium key parameters are also compared against established measures of geomagnetic activity, ionospheric currents, and other parameters governing solar wind/magnetosphere dynamics. These comparisons give additional verification of the physical correlation between the Iridium measurements and independent measures of geomagnetic activity and relevant solar wind quantities. Section 2 summarizes the Iridium magnetometer data preliminary processing. Section 3 describes the quantities we derive from the Iridium system data and covers their associated algorithms in detail. Section 4 presents comparison of Iridium observations with *Kp* and quick look (QL) *AE*, *AU*, and *AL*. Section 5 presents Iridium results for two geomagnetic storms together with the corresponding *Dst*, solar wind, and interplanetary magnetic field observations. The results are summarized and discussed in section 6.

2. Iridium System Data Preliminary Processing

[11] The preliminary data processing, including calibration corrections, model field subtraction, and baseline removal are discussed by *Anderson et al.* [2000]. A model for Earth's main field is evaluated at the satellite location in

the satellite along-track, cross-track, and nadir coordinates and subtracted from the data. The residuals are then cross-correlated with the model field using 24 hours of data to construct a matrix which is used to remove signals that correlate with the main field. This corrects for systematic gain, orientation, and cross-talk effects. Finally, as described by *Anderson et al.* [2000], long-period residuals are removed by zeroing the Fourier coefficients for periods longer than 26 min corresponding to 1/4 orbit. The 26 min period was found to be the longest period that gave no significant distortion of polar cap signatures. The resulting cross-track data are referred to as ΔB perturbations. The cross-track signals proved to be the most reliable because baseline variations are smallest in this component (the main field is approximately meridional) and the FAC signatures tend to be largest in the cross-track (nominally azimuthal) direction.

[12] The set of points having ΔB values above the noise level were identified using median statistics. The distribution of $|\Delta B|$ was constructed, and the median of this distribution was used to measure the intrinsic noise in the data. By examining a number of these distributions, the departure from a Gaussian distribution was found to occur at ~3.5 times the median of the distribution, and this factor was used to calculate a threshold level above which the ΔB were considered to be real signatures [*Anderson et al.*, 2000]. As shown by *Anderson et al.* [2000], the collection of points identified above threshold are concentrated at high latitudes; typically, <1% of points from middle to low latitudes are above threshold. Subsequent to *Anderson et al.* [2000], we found that the threshold increased with geomagnetic activity, indicating that the noise level was overestimated during active times. To standardize the thresholds, the geomagnetically quietest two or three days of each month from February 1999 through July 2000, a total of 52 days, were used to evaluate the background noise in the satellite data. The average of the thresholds for each satellite from this set of days is used as a threshold level for a given satellite. The set of thresholds has a median of 86 nT, a mean of 93 nT, a minimum of 68 nT, and a maximum of 210 nT (one satellite has a threshold above 155 nT).

[13] Figure 1 shows the results of this processing for data from the northern hemisphere for a 6 hour interval starting 31 July at 2000 UT. Blue, red, and gray dots indicate satellite locations in Altitude-Adjusted Corrected Geomagnetic (AACGM) coordinates [*Baker and Wing*, 1989] at times of magnetic field samples. (The green circle and yellow annulus are discussed below.) Eastward (westward) perturbations above threshold are color-coded blue (red). Points below threshold are plotted as gray dots. The most prominent feature of maps such as this (see also *Anderson et al.* [2000]) is the eastward (westward) perturbations in the evening (morning) organized in a ring at auroral zone latitudes consistent with the known statistical distributions of Birkeland currents [*Iijima and Potemra*, 1976a]. In addition, over the polar cap the perturbations are generally sunward (northern hemisphere) and appear as westward (eastward) in the evening (morning).

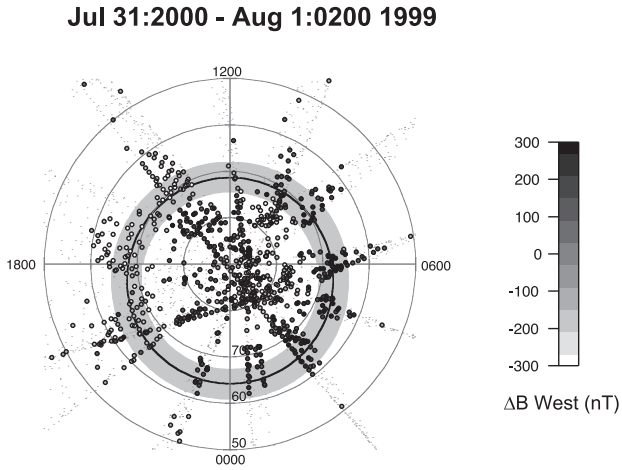

Figure 1. Polar view of Iridium system east-west magnetic perturbation data accumulated over a 6 hour period from 31 July to 1 August 1999. Data are plotted in Altitude-Adjusted Corrected Geomagnetic (AACGM) coordinates. Each magnetic reading is shown with gray, red, or blue dots, indicating measurements below threshold, westward above threshold, or eastward above threshold, respectively. The intensity of the colored dots reflects the magnitude of the perturbation. The green circle shows the least squares fit circle to the region 1/region 2 sense perturbations, and the yellow annulus indicates the range of radii that include 60% of the region 1/region 2 sense perturbations. See color version of this figure at back of this issue.

3. Summary Products

[14] Displays like Figure 1 give an overview of the systematic pattern present in the data but are inconvenient for surveying the time evolution of signatures in the data or for comparison with time series such as *AE*, *Kp*, or solar wind/IMF data. In addition, the maps do not provide quantitative measures of ΔB perturbations or their locations. We therefore developed procedures to derive measures of the intensity of the ΔB perturbations and the locations where the largest perturbations occurred. The definitions and algorithms used to calculate these summary products are the subjects of this section.

[15] Before giving the detailed discussion of each quantity, we give a brief overview of the entire set. First, we calculate the fraction of points detected above threshold in 2° latitude bins. The binning uses magnetic latitude, offset to the *Holzworth and Meng* [1975] average auroral center, which is a 3.1° shift toward the nightside on the noon-midnight meridian, and is denoted "offset MLAT." Second, the latitude distribution of the detected fraction is used to define the poleward and equatorward latitudes of samples above the detection threshold, denoted λ_E and λ_P. Third, we use data from the latitude range λ_E to λ_P to calculate the average eastward (positive) and westward (negative) ΔB values over the 95th to 100th percentile range. These are denoted as *dBE** and *dBW**, and the Net *dB* is defined as *dBE**−*dBW**. Collectively, *dBE**, *dBW**, and Net *dB* are denoted as Iridium indices because they are constructed by analogy with the familiar auroral electrojet indices, *AU*, *AL*, and *AE*. Finally, the points between λ_E and λ_P indicative of passage through the region 1/2 systems are used as input to a least squares procedure to fit a circle weighted by $|\Delta B|$. This fit is called the R12 fit and is the green circle shown in Figure 1. The yellow annulus in Figure 1 indicates the inner

and outer circles which contain 60% of the region 1/2 sense perturbations. It is determined by expanding (contracting) the circle until 20% of the perturbations lie at lower (higher) latitudes.

[16] The time window required to evaluate these quantities is determined by the rate at which data are accumulated by the constellation. It was chosen to be the minimum interval that contained enough data in a 2° latitude bin to give a measure of the detected fraction, nominally 10 samples. The typical sample interval for an individual satellite is 200 s [cf. *Anderson et al.*, 2000]. This corresponds to roughly 14° in latitude between samples. One therefore requires an average of seven passes of any of the Iridium satellites through a given latitude bin to acquire one sample per bin. Since there are six orbital planes (12 crossings through a given latitude bin) with 11 satellites in each plane (a time spacing of 9 min between satellites), there are 12 crossings of each 2° latitude bin every 9 min. Since on average one in seven crossings yields a magnetic field sample in a given 2° bin, the sample rate per latitude bin is roughly $12 \div 9 \div 7 = 0.2$ samples per minute. By this estimate it should take ~50 min to acquire 10 samples in a given 2° latitude bin. In practice, there are typically ~170 samples poleward of 60° latitude in each 45 min window, giving 11 points for every 2° of latitude. We therefore evaluate the summary products using a 45 min data window shifted in 15 min steps. We now discuss how each of the summary quantities is derived.

3.1. FAC Latitude Boundaries Determination

[17] The first step in calculating these quantities is to estimate the latitude range of Birkeland current perturbations because this latitude range determines the subset of points used in subsequent calculations. To do this, we considered the distribution of the fraction of points threshold versus offset MLAT. Examples of these distributions for three times from 31 July to 1 August 1999 are shown in Figure 2. The average detected fraction is used to measure the significance of peaks in these distributions. The average detected fraction is evaluated using bins with nonzero values poleward of 30° MLAT having at least five samples. Using only nonzero values in the average prevents data from low latitudes, where the detected fraction is often zero, from erroneously skewing the average. Requiring at least five points in a bin helps to guard against using statistically insignificant values. The detected fraction averages are given in each panel of Figure 2. In examining a number of cases, consistent enhancements in the polar regions correlated with average detected fractions higher than ~0.15. The threshold value of 0.15 ensures that roughly half of the bins have two points above the noise level, $2/11 = 0.18$, on average. (By definition, the lowest possible average detected fraction is 0.09 on average since zeroes are excluded.) The dashed lines in Figure 2 are at a detected fraction of 0.15.

[18] The equatorward and poleward latitude boundaries, denoted λ_E and λ_P, respectively, were determined as follows. If the average detected fraction was <0.15, λ_E and λ_P were set to default values of 70° and 90°, respectively (negative in the south). Setting a minimum average reduces spurious effects due to random points above the noise level which would otherwise corrupt the results for low levels of geomagnetic activity. Since the purpose of this latitude range is merely to restrict further analysis to points lying between λ_E and λ_P, the exact choice for the default range is not critical.

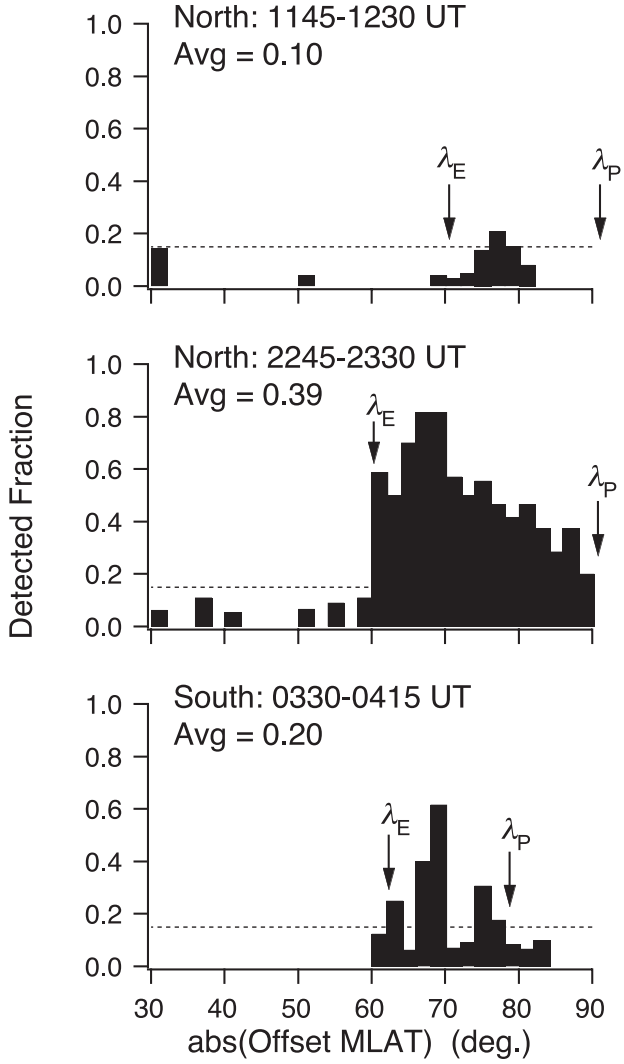

Figure 2. Histogram distributions of the fraction of samples with $|\Delta B|$ above the noise threshold versus offset MLAT in 2° bins for three intervals from 31 July to 1 August 1999.

[19] If the average detected fraction was >0.15, the following algorithm was used. The equatorwardmost point having a value exceeding the average was located. Then the last point equatorward of this having a value above 0.15 was identified as the equatorward boundary. The poleward boundary was defined in the same way by locating the polewardmost point with a value exceeding the average and then finding the last point poleward of this with a value above 0.15. Boundaries for the southern and northern hemispheres were evaluated separately.

[20] The results of this algorithm are indicated by the arrows in Figure 2. In the 31 July, 1145–1230 UT period the average was below 0.15, so the default range was used. For 31 July, 2245–2330 UT the equatorward boundary coincides with the first point having a value below 0.15. The poleward boundary was 90°. The final case, taken from the southern hemisphere, illustrates why the algorithm starts

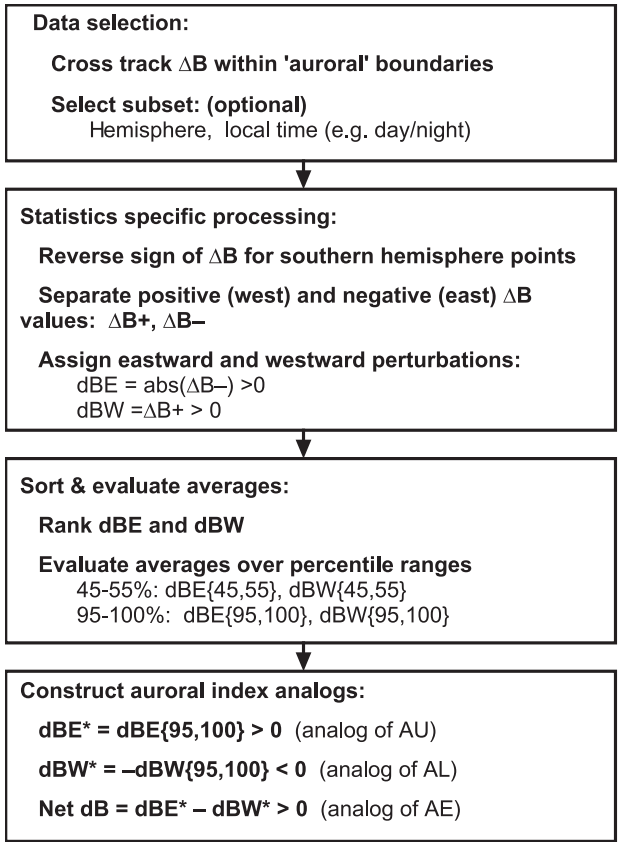

Figure 3. Calculation steps used to calculate the Iridium Birkeland current indices constructed to be analogous to the conventional auroral electrojet indices. See text for details.

searching with the most equatorward or poleward point having a value above the average. Since the 1 August, 0330–0415 UT distribution has two "holes" in it, an algorithm that simply started from the maximum and looked for the first point below the average would have chosen too narrow a range.

3.2. FAC Intensity Indices

[21] The data between λ_E and λ_P were then used to obtain the Iridium indices, *dBE**, *dBW** and Net *dB*. Figure 3 shows the steps in their calculation. The calculation uses all of the data between λ_E and λ_P. If a subset of the data is to be used, for example, only the nightside, the subset of data is extracted. Several manipulations are then required to account for the hemisphere and to correlate with conventional auroral electrojet indices. In the northern hemisphere the eastward (westward) ΔB in low-Earth orbit above the ionosphere corresponds approximately to eastward (westward) Hall current or positive (negative) *H* perturbation on the ground and is analogous to *AU* (*AL*). In the southern hemisphere the ΔB observed at Iridium altitude is reversed relative to the northern hemisphere, so for purposes of constructing these Iridium indices, the sign of ΔB values obtained from the southern hemisphere is reversed. We then separate positive points, $\Delta B+$, from negative points, $\Delta B-$. Since negative ΔB is eastward (see Figure 1), we construct the data subsets *dBE* and *dBW* as shown in Figure 3 so that all of the *dBE* and *dBW* are positive. The *dBE* and *dBW* subsets are then sorted separately and averaged over two percentile ranges: 45–55 and 95–100. The 95–100 percentile averages are denoted *dBE** and *dBW**. Averaging over the top 5 percentile was used to emulate the envelope technique used to construct the auroral electrojet indices. The median of the distribution, 45–55%, is used to give a sense of the main body of the distribution. The indices are then assigned as shown in Figure 3. The *dBW** are reported as negative values so that *dBE** and *dBW** are analogous to *AU* and *AL*, respectively. The difference, *dBE** − *dBW**, is denoted Net *dB* and is analogous to *AE*.

3.3. Region 1/Region 2 Fit Parameters

[22] In addition to the latitude limits λ_E and λ_P, it is of interest to identify more precisely the latitude where the Birkeland current perturbations maximize. To do this, we fit a circle to the points whose perturbations indicate passage through the region 1/region 2 currents shown as a green circle in Figure 1. It is called the R12 fit. Both the center and radius of the circle are free parameters. Figure 4 shows the steps and quality checks used to guard against erroneous results. The fit uses the data between λ_E and λ_P, but we remove the points whose $|\Delta B|$ are below the noise threshold of each satellite. We then assign Cartesian coordinates to

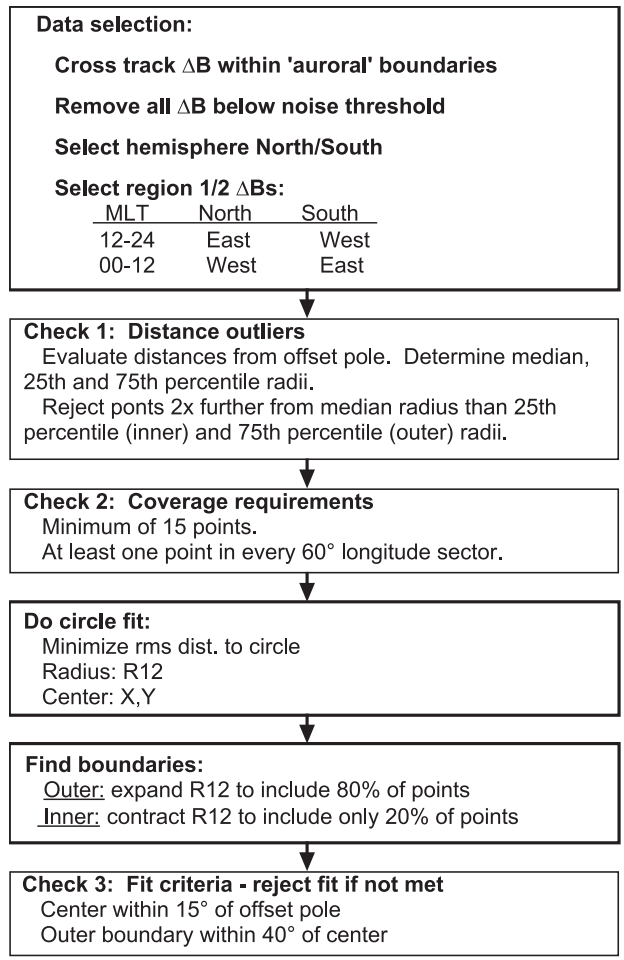

Figure 4. Calculation steps and quality checks used for determining the circle fit to region 1/region 2 sense magnetic perturbations. See text for details.

data point locations in units of colatitude degrees using the MLT and MLAT of each point.

[23] We select those points indicating passage through the region 1/2 current systems as follows. In the northern (southern) hemisphere these are eastward (westward) in the evening and westward (eastward) in the morning. For this purpose we assume that the noon midnight meridian is the dividing plane between dawnside and duskside region 1/2 systems. This choice occasionally excludes points near noon and midnight, for example, westward in the morning northern hemisphere, that are legitimately part of the global FAC system. This is a small fraction of the local time span of the region 1/2 signals, however, and their exclusion does not have a major impact on the fit. During quiet times the perturbations move to high latitudes on the dayside. When this happens, the distributions of points fail the local time distribution test because they are all on the dayside.

[24] Two checks are performed to ensure that the distribution of points used in the fit does not deviate in obvious ways from the assumed region 1/2 distribution. The first quality check rejects outliers from the region 1/2 data subset. This is done by evaluating the distances of all points from the offset pole (shifted toward midnight by 3.1°). These distances are then ranked, and the distance from the pole to the median, 25th and 75th percentiles are calculated. Points that lie twice as far beyond the median as the 75th percentile or twice as far inside the median as the 25th percentile are rejected. This check was developed by experience and accomplishes two things: (1) it rejects spurious low latitude points that would otherwise seriously distort the fit; and (2) it rejects most large polar cap perturbations that have the same sense as the region 1/2 perturbations.

[25] The second quality check is imposed to ensure that the circle fit is constrained with points at all local times. First, we require that the fit use at least 15 points. Second, we require that points be well distributed in longitude. We use two sets of 60° wide longitude sectors, one in which midnight is a boundary between sectors and the other in which a sector is centered on midnight. We require that there be at least one point in each 60° longitude sector in both sets of sectors. Using only one set of longitude sectors permits the possibility of a 120° longitude gap between points. Such a large gap inadequately constrains the least squares circle fit, allowing it to expand to unreasonably low latitudes in regions without samples. Using two sets of longitude bins ensures that the largest allowed longitude gap is 60° and eliminates this problem. If by these checks the fit is not applicable, it is not done.

[26] The circle fit uses a simplex algorithm [*Press et al.*, 1987] with three free parameters, the coordinates of the center and the circle radius. The fit minimizes the sum of the squares of the shortest distances to the circle, weighted by $|\Delta B|$. The error function is the sum of the squares of the difference between the circle radius and the distance between the circle center and each point. The terms in the error function are weighted by the $|\Delta B|$ for each point. The R12 center and radius are determined by minimizing the error function. Circle fit radii are reported in degrees colatitude.

[27] The latitude extent of region 1/2 perturbations is also estimated. The yellow annulus in Figure 1 shows the range of radii centered on the R12 fit which include 60% of all region 1/2 sense perturbations. This is done by ranking the distances between the circle center and the data. The 20th and 80th percentiles determine the inner and outer boundaries, respectively. The difference between the inner and outer boundary radii provides a measure of the latitudinal extent of the current systems.

[28] One quality check is performed after the fit. The fit is rejected either if the center is more than 15° from the offset pole or if the outer boundary radius is larger than 40°. The latter restriction does reject a few legitimate fits during highly disturbed times, but the number of erroneous fits rejected during quiet times more than compensates for this known problem. In the worst case so far, 5 of 720 fits were rejected during a 24 hour period during the 15–16 July 2000 storm. As needed, these cases can be rerun without the restriction on the outer boundary.

3.4. Summary Products: Example Case

[29] Figure 5 shows the summary products for the 24 hour period beginning 31 July 1999 at 0800 UT. The gray scale plots show the detected fraction versus latitude and time for the northern (Figure 5a) and southern (Figure 5b) hemispheres. The detected fraction is plotted with 1.0 as black and 0.0 as white. The black traces in Figures 5a and 5b show λ_E and λ_P for both hemispheres. The λ_E and λ_P traces are only plotted when values other than the defaults are used. The R12 centroid and inner/outer boundaries are overlaid in white on the detected fraction gray scale displays. Figure 5c shows Net *dB*. Figures 5d and 5e show *dBE** and *dBW** (negative values) for the dayside and nightside.

[30] For the interval shown in Figure 5, a close correspondence is seen between the latitudes of FAC locations and their intensities. A period of low-level fluctuations and few points detected above threshold, 0800–1600 UT, is followed by an increase in the points above threshold, an expansion of R12, and an increase in Net *dB*. Birkeland current perturbations extend equatorward of 60° in both hemispheres, and R12 expands from 75° to almost 65° MLAT. The perturbation signatures also increase in intensity with Net *dB* reaching over 800 nT near 2100 UT and again just after 0000 UT. After 0500 UT the fraction of points above threshold drops, as do the Iridium indices. On the dayside the *dBE** and *dBW** are comparable, while on the nightside, *dBW** tends to dominate.

[31] The correlations between the parameters shown in Figure 5 are all consistent with expectations for the Birkeland FAC system. Overall, the northern hemisphere shows a higher fraction of detected points, consistent with a higher ionospheric conductivity and hence larger currents in the northern hemisphere at this time of year. Even so, the two hemispheres show similar dynamic variations in R12 and their detected fractions. The Iridium index patterns are also qualitatively consistent with expectations; the currents intensify as the auroral oval expands, and the *dBW** (*AL*) signature dominates on the nightside.

[32] Finally, we found instances in which spurious index or fit results were obtained. This generally happens when there are very few auroral perturbations, as occurs during quiet periods. In that case, noise in low-latitude regions can occasionally corrupt the auroral boundary and index calculations. These cases are easily recognized as anomalous equatorial auroral boundary points immersed in a time series of high-

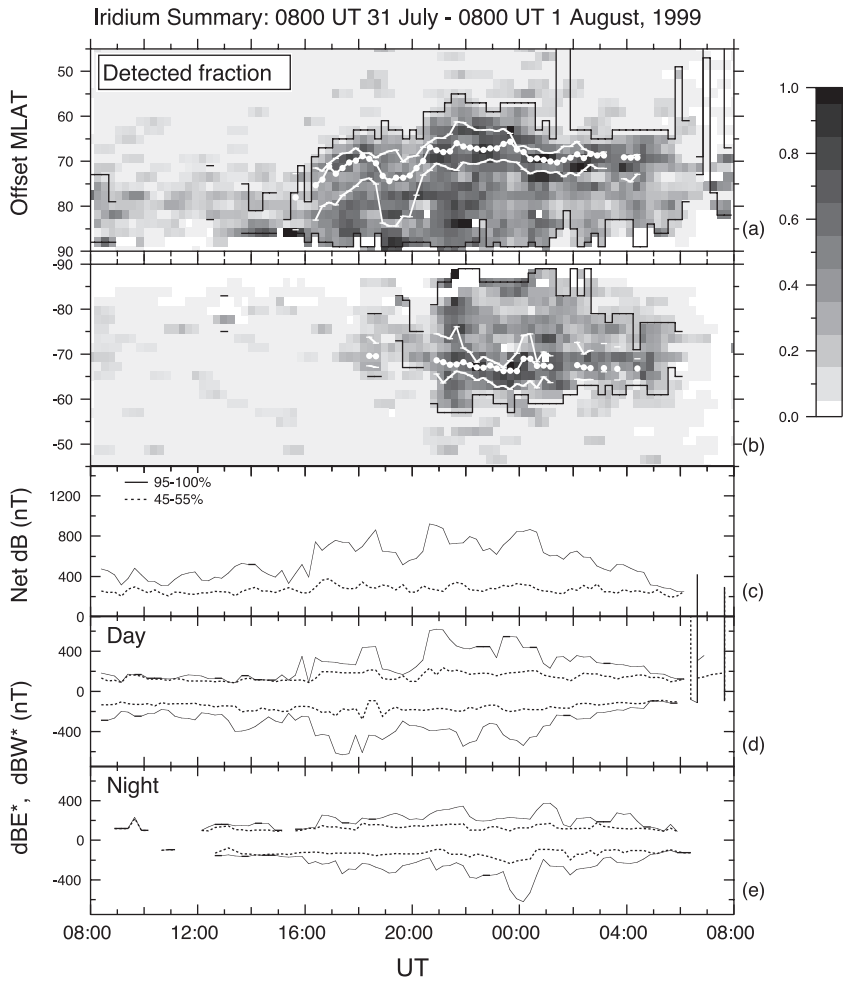

Figure 5. Summary products from Iridium data for a 24 hour period from 0800 UT on 31 July to 0800 UT on 1 August 1999. Figures 5a and 5b show the relative fraction of measurements detected above threshold in 2° MLAT bins. Circles of latitude are offset toward midnight by 3.1° to be better centered on the statistical auroral oval. In Figures 5a and 5b the white traces with dots show the R12 center radius, and the traces with dash markers show the upper (80%) and lower (20%) percentile radii of the oval fit. Figures 5c–5e show the percentile bin averaged perturbations, ΔB, for data obtained on the (c) dayside, (d) nightside, and (e) maximum minus minimum eastward perturbation. Solid lines show the 95–100% average, and dashed lines show the 45–55% average.

latitude boundaries. To remove these bad fit results, monthly summary statistics were surveyed visually and erroneous values were removed manually using an interactive display tool. Manual inspection is not applied to the daily survey products shown in Figure 5, but the data used for comparison with quick look auroral electrojet indices and *Kp* presented below were the cleaned monthly summary statistics.

4. Ground Comparison

[33] Comparing the Iridium and auroral electrojet indices serves to check whether the Iridium signals are primarily a physical signal associated with auroral currents. For the same electric field and ignoring geometrical effects, the ground signals are proportional to the Hall conductivity, whereas the Birkeland currents would be proportional to the Pedersen conductance. Since the conductivity ratio varies in both space and time, the space and ground perturbations will not have a fixed ratio. Finally, since only quick look (QL) indices are available for the relatively recent Iridium data (since February 1999), we must bear in mind that the ground station coverage is not as extensive as for the final auroral electrojet indices. Quick look values are indicated by *, for example, *AE**. Nonetheless, the QL and Iridium indices should be statistically well correlated if they respond to the same electrodynamic system.

[34] The QL indices used here are 1 min values from the period February through September 1999. During this period nine stations were usually reporting, but occasionally reports were not available from one, two, or three stations for a few hours at a time. The minimum number of stations used was six. The raw QL indices contain spikes which were removed as follows. We first constructed histogram distributions of differenced values for each QL index using a 3 hour interval, ~180 points. The width of the distribution, δ, was calculated as the spread of values from the 10th

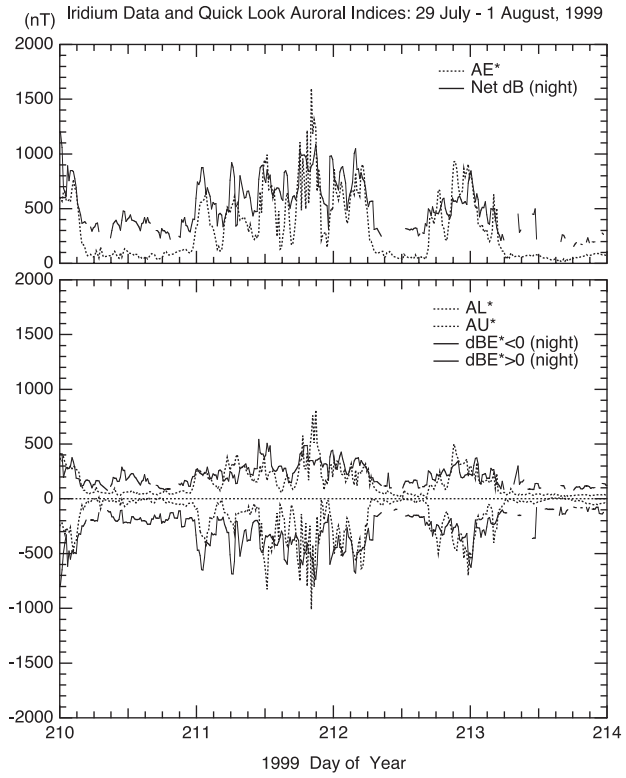

Figure 6. Quick look auroral electrojet indices *AE**, *AU**, and *AL** together with Iridium-derived Net ΔB, positive eastward ΔB, and negative eastward ΔB averaged over the 95–100% percentile range for a moderately quiet 4 day period in September 1999. Iridium ΔB were calculated using nightside data.

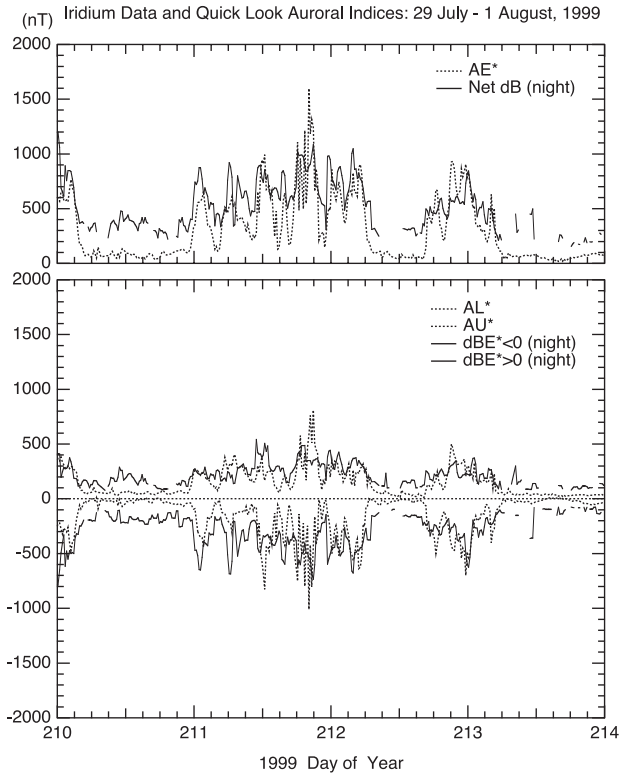

Figure 7. Quick look auroral electrojet indices and Iridium-derived ΔB for a 4 day period beginning 29 July 1999 in the same format as Figure 6.

to 90th percentile ranked by QL index value. Points lying more than 5δ away from the median were discarded and replaced by points linearly interpolated in time between nearest valid neighboring points. Quantities were calculated from the Iridium data using 45 min windows, so for comparison with the QL indices we used the 1 min QL value nearest the center of the 45 min Iridium window.

[35] Figures 6, 7, and 8 show Iridium and auroral QL indices for three representative days. The correlation between Net *dB* and the *AE** is slightly higher for the Net *dB* derived from nighttime Iridium data (shown below), so we use Iridium indices derived from nightside data in these plots. Figure 6 shows data from a period of low to moderate activity. On 2–5 September 1999 the provisional *Dst* ranged between −27 nT and +2 nT. The average *Kp* for 2, 3, 4 and 5 September were 2.1, 2.8, 2.5, and 1.4, respectively, with a maximum *Kp* of 4o for 0600–0900 UT on 3 September. The last geomagnetic storm before this period was on 23 August. The *AE** occasionally exceeds 500 nT, and when it does, the Net *dB* is enhanced as well. Intervals for which *AE** remains below 100 nT are also the times of lower Net *dB*. The *AU** and *AL** are similarly correlated with *dBE** and *dBW**, respectively. The lower limit for *dBE** is 100–200 nT (similarly, $dBW^* \leq -100$ to −200 nT), reflecting the fact that the values are averaged over the highest 5% of a data set with an inherent resolution limit of 48 nT. As a result, the Net *dB* rarely falls below 300 nT, even for quiet conditions.

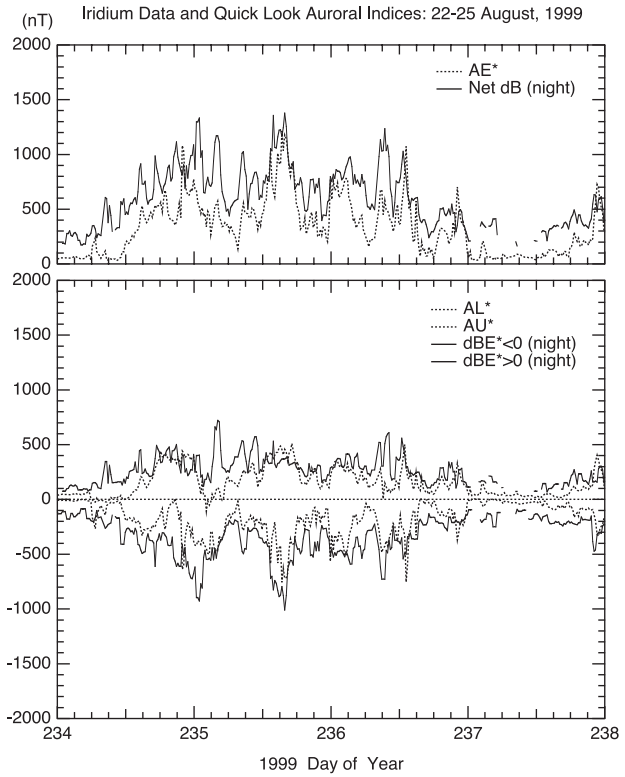

Figure 8. Quick look auroral electrojet indices and Iridium derived ΔB for a 4 day period beginning 22 August 1999 in the same format as Figure 6.

[36] Figure 7 shows Iridium and auroral QL indices for 29 July through 1 August 1999. This is a period of a small storm, with a SSC at 1827 UT on 31 July and a minimum $Dst = -60$ nT at 0200–0300 UT on 31 July. The average Kp were 1.5, 4.4, 3.6, and 1.5 for the 29th, 30th, 31st, and 1st, respectively. The maximum Kp of 8- occurred at 1800–2100 UT on 30 August. A correlation between the Iridium and QL auroral electrojet indices is more evident in this case. The periods of enhanced AE^* are early on the 29th (day 210), from the beginning of the 30th (day 211) through ~0700 on the 31st (day 212), and again from 1600 UT on the 31st to 0400 UT on the 1st. On day 211, AE^* and Net dB display similar temporal profiles, and although some of the shorter duration peaks do not match, for example, the spike in AE^* just before 2100 UT, the 1–3 hour timescale variations agree quite well.

[37] Figure 8 shows data from 22–25 August 1999, during which a moderate storm occurred. The Dst minimum was −80 nT at 1500–1600 UT on the 23rd, and the maximum Kp was 6- for 0000–0300 UT on the 23rd. The average Kp were 2.1, 4.1, 4.0, and 1.9 for the 22nd, 23rd, 24th, and 25th, respectively. There is general agreement in the temporal profiles for AE^* and Net dB. Even though the relative magnitude of the peaks varies, the 1–3 hour timescale peaks tend to occur at the same times.

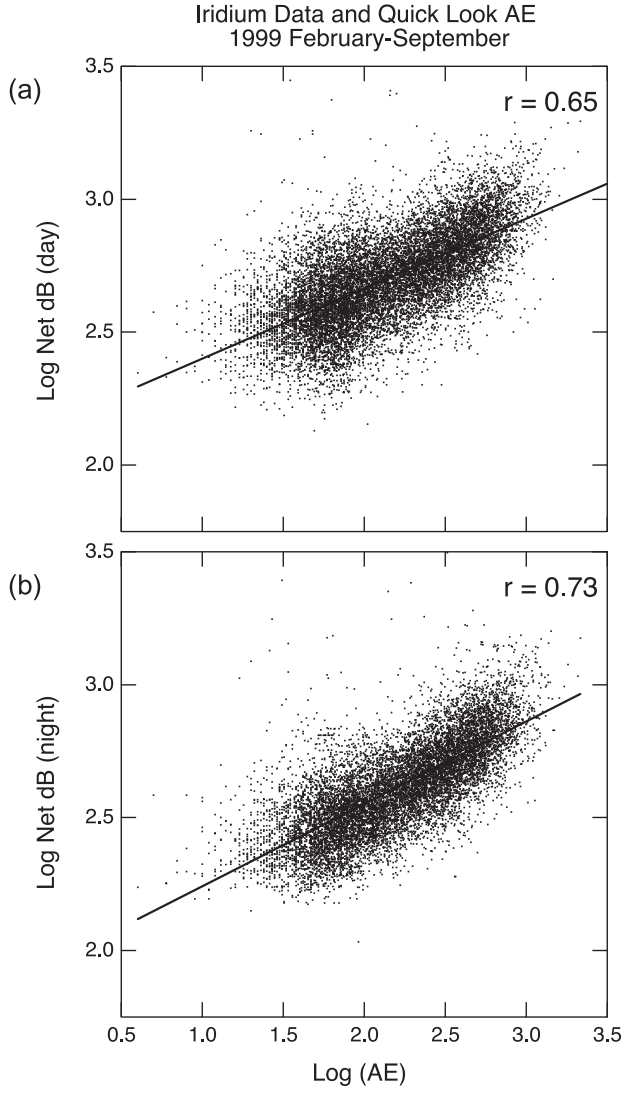

Figure 9. Scatterplot of the Iridium net ΔB (95–100%) against the QL auroral index, AE^*, for (a) dayside and (b) nightside Iridium data. Linear fits to the log values are also shown together with the regression coefficients.

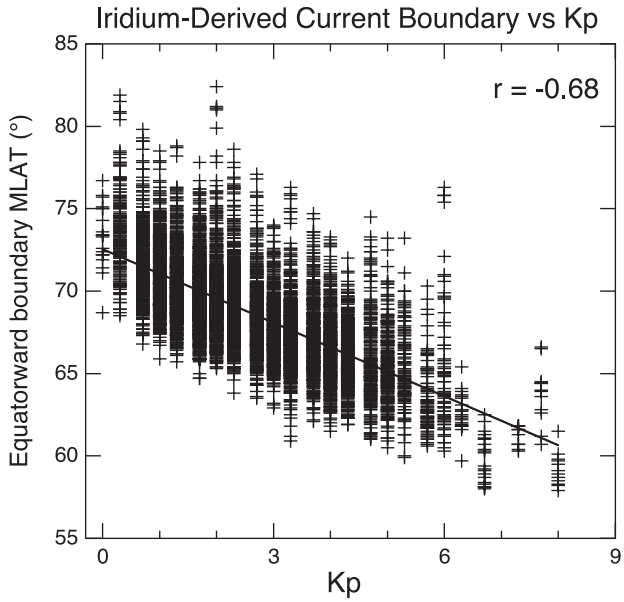

Figure 10. Scatterplot of the equatorward R12 boundary (derived as described in the text) and the Kp index together with the linear fit and regression coefficient.

[38] Figure 9 shows log(Net dB) versus log(AE^*) for the February–September 1999 period. Figure 9a (Figure 9b) uses the Net dB from the dayside (nightside). The correlation between log(AE^*) and log(Net dB) is fairly good in both cases, 0.65 and 0.73 for dayside and nightside Iridium data, respectively. On average, the QL auroral zone stations are positioned under the electrojet somewhat better at night than during the day, possibly accounting for the slightly better correlation with the nightside Iridium data. In any case, the correlation confirms the impressions from the examples that the perturbations derived from the Iridium system are closely related to the current system driving the auroral electrojets.

[39] Finally, we examined the correlation between R12 and Kp to see whether this parameter reflects the general state of magnetic activity. Figure 10 shows the equatorward boundary of R12 versus Kp for February–September 1999. The linear regression coefficient is −0.68, reflecting the tendency of the auroral oval to expand equatorward with increasing Kp. For $Kp < 3$ the equatorward R12 boundary continues to retreat poleward, indicating that even though the resolution of the Iridium magnetometers is relatively low, the statistical ensemble still yields information about the location of the large-scale currents for low to moderate activity.

5. Storm Behavior

[40] The Birkeland current system should display clear dynamics during geomagnetic storms, and this should be reflected in the Iridium data. The currents should intensify and should expand equatorward at the onset of storm main

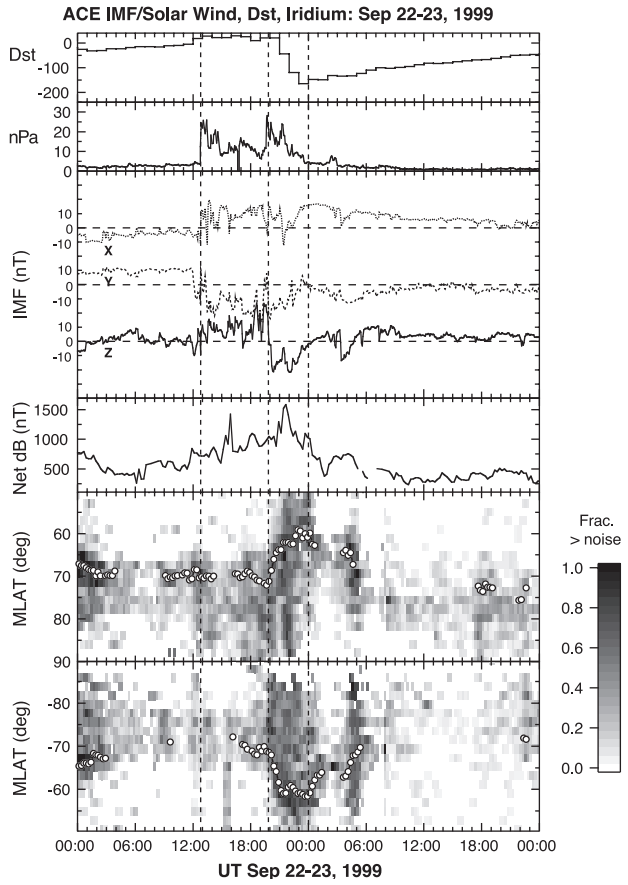

Figure 11. (top) *Dst* index, (second panel) solar wind ram pressure from ACE SWEPAM, (third panel) interplanetary magnetic field from ACE MAG, and Iridium system derived parameters, (fourth panel) ΔB net, and (bottom panels) fraction detected and R12 fit latitude for the northern and southern hemispheres for 22 and 23 September 1999. In the bottom panels, gray scales span the range from 0 (white) to 1 (black), while open circles indicate the R12 MLAT for the 45 min window centered on the time for which the points are plotted.

phase, and there may be a close relationship between the Birkeland currents and the interplanetary magnetic field (IMF). We present results for two storms, 22–23 September 1999 and 21–22 October 1999, to check these expectations.

5.1. The 22–23 September 1999 Storm

[41] The provisional *Dst*, solar wind, and IMF from the Advanced Composition Explorer (ACE) spacecraft and Iridium results for the 22–23 September storm are shown in Figure 11. The ACE data have been time lagged to Earth assuming simple convection from the L1 point using the solar wind speed. Vertical dashed lines indicate changes in the solar wind of greatest importance here. The maximum *Kp* for this storm was 8o for 2100–2400 UT on the 22nd, and *Kp* stayed above 5o for 12 hours from 1800 UT on the 22nd through 0600 UT on the 23rd. This was a major storm with a minimum *Dst* = −160 nT. The initial phase of the storm began with a sharp increase in solar wind pressure from 4 to 25 nPa shortly after 1200 UT on the 22nd (day 265) and is associated with a positive jump in *Dst*. This was followed 9 hours later by rapid *Dst* decrease, corresponding to a short main phase.

[42] An increase in the solar wind ram pressure from 10 nPa to over 20 nPa occurs shortly after 2000 UT and is followed by a B_z north to south turning. The southward turning coincides with main phase onset. The IMF B_z component reaches −20 nT twice during the main phase. The recovery phase begins when the IMF becomes nearly radial, $B_z \sim 0$ nT, at ~0000 UT on the 23rd. At this time the solar wind pressure decreases below 5 nPa. There is another interval of southward B_z from 0300 to 0430 UT on the 23rd, but B_z remains positive or close to zero, and the IMF magnitude is below 10 nT for the remainder of the day.

[43] The Net *dB*, detected fraction, and R12 fit latitude (for the north and south) are shown in the bottom three panels of Figure 11. The Net *dB* ranges from 300 nT to 750 nT before the storm initial phase. At storm initial phase the Net *dB* increases somewhat from 500 to 750 nT and continues to increase through the initial phase with a brief peak over 1250 nT around 1600 UT on the 22nd. The R12 latitude and the detected fraction remain fairly steady through the initial phase. At main phase onset the R12 latitude changes by ~8°, corresponding to an equatorward expansion of the Birkeland current system in both hemispheres. The maximum Net *dB* of 1500 nT occurs shortly after this initial expansion. The R12 latitudes reach their most equatorward values of ~60°N and S near 2300 UT on the 22nd. The R12 latitude begins retreating poleward at 0000 UT, coincident with the beginning of the recovery phase. There is a noticeable decrease in the detected fraction from about 0130 to 0300 UT, and there are not enough points to allow a R12 fit during this time. At 0300 UT the detected fraction increases again, and there are enough points to make R12 fits. The currents retreat poleward as the IMF B_z decreases from 0300 to 0430 UT, and the detected fraction drops to quite low levels again. The Net *dB* remains below 500 nT for the remainder of the day.

[44] The Iridium results are therefore closely related to the dynamics indicated by *Dst* and the IMF. That the currents are not small during the initial phase but are actually enhanced is attributed to the strong IMF B_y, B_y = −10 to −20 nT, which may be strong enough to drive magnetospheric convection despite the northward B_z. Nonetheless, the Birkeland currents do not expand equatorward until B_z turns southward, and then the equatorward expansion is rapid, 8° in ~1 hour. The currents remain at low latitudes throughout the southward B_z interval but retreat poleward in association with the northward turning. The brief southward IMF turning coincides with a reappearance of enhanced Net *dB* and detected fraction.

5.2. The 21–22 October 1999 Storm

[45] Data for the 21–22 October storm are shown in Figure 12 in the same format as Figure 11. This storm is less classic in its *Dst* profile and was associated with a more complex series of events in the solar wind and IMF than the 22–23 September event. The *Dst* time evolution does not have a clear initial phase, has a more gradual storm main phase from 0000 to 0600 UT on the 22nd (day 295), and reaches a deeper *Dst* minimum, −230 nT. The maximum *Kp* was 8o from 0600 to 0900 UT on the 22nd, and *Kp* remained above 5o for 12 hours, 0000–1200 UT on the 22nd.

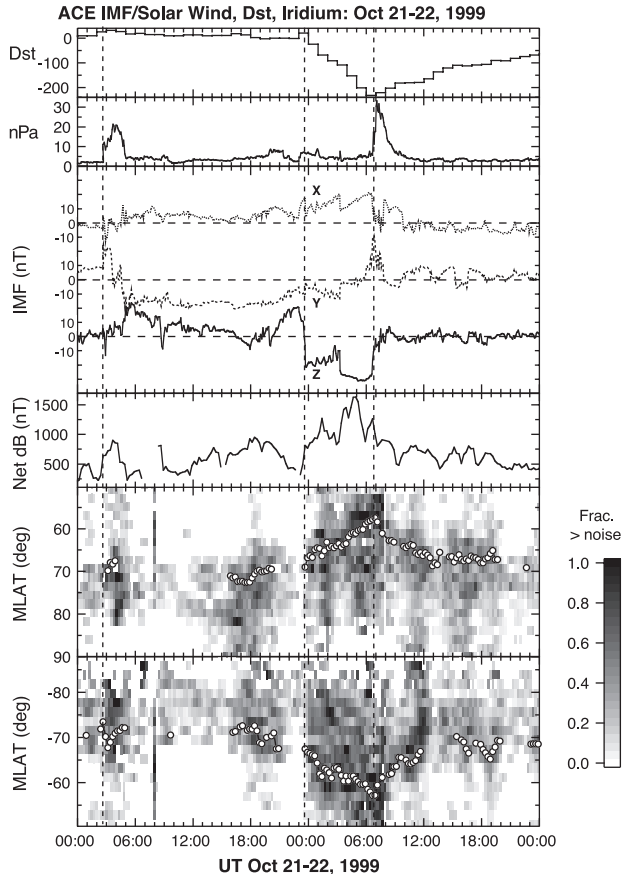

Figure 12. *Dst*, solar wind, IMF, and Iridium results in the same format as Figure 11 for the 21–22 October 1999 storm.

[46] The solar wind feature is bracketed by two solar wind density enhancements, giving large, order of magnitude pulses in dynamic pressure. The first pressure pulse arrives at 0300 UT on the 21st, lasts for ~2 hours, and has a dynamic pressure of slightly over 20 nPa. The second occurs from 0700 to 0900 UT on the 22nd and has a peak pressure over 30 nPa. In between, the IMF magnitude ranges between 20 and 30 nT and executes a variety of rotations. Initially, at 0300 UT on the 21st, the IMF is almost purely positive B_y, but after the first pressure pulse it turns northward with a strong negative B_y. The negative B_y is sustained at −15 nT to −20 nT from 0500 to 2100 UT on the 21st, while B_z decreases from +20 nT initially to ~5 nT from 1030 to 1600 UT and then varies between +5 nT and −5 nT to 2100 UT. At ~2100 UT B_z becomes positive and is the dominant component. Shortly before 0000 UT on the 22nd, B_z executes a sharp reversal from +20 nT to −20 nT, coincident with main phase onset. At 0300 UT, B_z abruptly becomes more negative and reaches −30 nT shortly after 0500 UT. Coincident with the second large pressure pulse around 0700 UT, the IMF magnitude decreases, and B_z rises abruptly to between −10 and 0 nT. During the rotation the IMF sweeps through strong positive B_y. By 0800 UT the B_z component turns positive and remains relatively small, varying between positive and negative for the remainder of the day. From 0800 to 1800 UT the IMF is alternately dominated by the B_x or B_y components, with generally strong positive B_y.

[47] The signals recorded by the Iridium system closely parallel storm development and the variations in the IMF. The initial pressure pulse corresponds to a brief increase of the Net *dB* up to almost 1000 nT and an intensification in the detected fraction from 0300 to 0400 UT on the 21st. Despite the enormous increase in pressure, the R12 latitude is ~70° in both hemispheres. The intense currents may be due to the intense IMF B_y, +20 nT with a very small B_z. From 0500 to 1200 UT the Net *dB* is low, below 400 nT (except for a spike around 0800 UT which is probably associated with contamination perturbations which are attributed to satellite operations). The detected fraction remains low in both hemispheres until ~1600 UT, corresponding to the period of positive IMF B_z. The IMF decreases somewhat irregularly from 0600 to 1600 UT, and from 1200 to 1600 UT the Net *dB* and detected fraction display variability as well. The period when the IMF B_z actually turns southward from about 1600 to 2000 UT on the 21st corresponds fairly closely to a sustained enhancement in Net *dB* to slightly more than 750 nT and a significantly increased detected fraction. In the final four hours before main phase onset, the Net *dB* decreases, and the detected fraction is low.

[48] Coincident with main phase onset and the abrupt IMF B_z southward turning at 0000 UT on the 22nd, the Net *dB* jumps to ~700 nT, and the detected fraction suddenly increases over a broad range of latitudes. The R12 latitude indicates a first appearance at ~68°. As B_z remains southward, Net *dB* and the detected fraction remain high and R12 displays a progressive expansion to lower latitudes. When B_z becomes even more negative at 0300 UT on the 22nd, the Net *dB* jumps to over 1000 nT, maximizing at 1600 nT. Meanwhile, R12 continues to change, indicating expansion of the Birkeland currents below 60° MLAT by 0600 UT. Even though R12 remains below 60° for the last hour of strongly southward IMF B_z, the Net *dB* decreases to ~1000 nT. At 0400 UT on the 22nd, when the second pressure pulse arrives and the IMF intensity drops coincident with a change in direction, initially duskward and then earthward, Net *dB* decreases to ~750 nT and R12 displays a prompt retreat poleward. From 0500 to 1300 UT, R12 continues a gradual poleward retreat, while Net dB remains between 400 nT and 600 nT. Even though B_z is not southward and the auroral zone appears to retreat poleward, the Birkeland currents appear to be sustained. During the 1300–1900 UT period, R12 holds between 68° and 70° with Net *dB* near 500 nT. At the same time, *Dst* holds steady or decreases slowly. After 1900 UT the IMF is more nearly radial, the IMF B_x is greater than B_y, so that the field in the *Y-Z* GSM plane is quite small. During this time the Net *dB* falls below 500 nT, and the detected fraction is markedly diminished.

6. Discussion

[49] These comparisons of parameters derived from the Iridium system engineering magnetometer data with familiar auroral electrojet indices indicate that the Iridium system data provide measurement of the global Birkeland current system. There are good correlations between the Net *dB*, *dBE**, and *dBW** parameters and quick look *AE*, *AU*, and

AL, respectively, for individual events and statistically for Net *dB* and quick look *AE*. There are several reasons we do not expect a perfect correlation. First, the ground stations used for the QL indices have limited spatial resolution and coverage. Second, the Iridium data have limited temporal and longitude resolution, so that the Iridium signals will most likely miss current systems that correspond to FACs that are either localized or occur rapidly, such as substorm onsets. Finally, the parameters measure different current systems which are linked by the Hall to Pedersen conductivity ratio, which is variable in both time and location. Because of this combination of factors, we cannot at this time identify the sources of residual disparity between the Iridium results and the QL indices, and we caution against reading more into these correlations than can properly be concluded. What we can conclude is that the good correlations between ground and Iridium magnetic signatures indicate that the dBE* parameters primarily reflect a real physical signature of the system that is also responsible for the magnetic signatures on the ground. The correlation of the equatorward limit of R12 with *Kp* is consistent with expectations that the auroral zone and hence the Birkeland currents generally expand equatorward with increasing geomagnetic activity.

[50] The results for the two storms considered here show a close link between the IMF and the FAC current intensity and equatorial expansion. Enhancements in Net *dB* and the detected fraction appear to respond directly to the IMF intensity and orientation. The strongest Net *dB* and the highest and broadest detection fractions occur during the most intense southward IMF, and the lowest Net *dB* and weakest detected fraction occur during northward IMF. The periods of strongest Net *dB* and most equatorward R12 correspond to the storm main phase in both instances. Storm recovery is associated with decrease in Net *dB* and the retreat of R12 poleward. The rapid recovery for the 22–23 September storm corresponds to prompt decrease in Net *dB* and poleward retreat, whereas the more gradual, stepped, *Dst* recovery for the 21–22 October storm corresponds to a gradual poleward retreat of R12 and sustained Net *dB* above quiet levels. In addition, the northern and southern hemisphere detected fractions and R12 fits display similar intensifications and time development. Finally, we note that periods of small IMF B_z but for which the IMF B_y component is dominant yield significant Net *dB* and that sustained values for R12 correlate with a more gradual recovery of *Dst* than when the IMF turns strongly northward.

[51] The Iridium system data provide new insight into the evolution of the Birkeland current system through the course of these storms. For the September storm the sudden southward IMF turning occurs as the solar wind dynamic pressure increases sharply and the FACs expand equatorward by 10° in 1.5 hours and expand another few degrees while the IMF remains southward. The mean latitude of the region 1/region 2 system reaches 58° MLAT. In the October storm the IMF southward turning at main phase onset is just as sharp but occurs during a period of nominal dynamic pressure, and rather than a sudden equatorward expansion of the FAC system, the currents expand progressively equatorward 13° over ~8 hours of sustained southward IMF with B_z reaching −30 nT. The mean region 1/region 2 latitude reaches 56° in this storm. In both storms the current intensity decreases to prestorm levels or below within an hour when the IMF turns northward or nearly horizontal, at the beginning of storm recovery. The poleward retreat of the currents also begins promptly when the IMF turns northward but takes longer, roughly 6 hours in both cases. These results suggest that the IMF is the dominant factor in determining the intensity of the currents but that the expansion and contraction of the auroral oval is determined also by the time history of the IMF and more promptly by the solar wind dynamic pressure, provided the IMF is southward.

7. Summary and Conclusions

[52] This paper presents techniques developed to derive measures of the globally distributed Birkeland current magnetic signatures recorded by the engineering magnetometers of Iridium satellite constellation. The parameters of greatest utility are the maximum eastward and westward perturbations, *dBE** and *dBW**, the net magnetic perturbation, *dBE** − *dBW** = Net *dB*, the centroid of the region 1/region 2 currents, R12, and the fraction of points detected above the noise threshold. The *dBE** and *dBW** are the average over the 95–100% range of the most positive and negative eastward perturbations analogous to *AU* and *AL*, respectively, with the obvious difference that *dBE** corresponds to the Birkeland currents, whereas *AU* and *AL* measure the ionospheric Hall electrojet currents. The Net *dB* is analogous to *AE*. The R12 parameter is the radius of the centroid of samples corresponding to points representing the nominal perturbations expected when the satellites are traversing the region 1/region 2 current systems. It is determined by a least squares fit of the points having region 1/region 2 sense perturbations and is weighted by the magnitude of the perturbations. The latitudinal extent of the region 1/region 2 sense perturbations is measured by the colatitude radii having the same center as the R12 fit that encompass 20% (inner) and 80% (outer) of the region 1/region 2 sense perturbations. The fraction of points above threshold is evaluated over all longitudes in 2° magnetic latitude bins and is the ratio of points above the noise level to the total number of samples. The noise level for each Iridium satellite was determined from an ensemble of 52 days corresponding to the quietest days of each month for the period from February 1999 through July 2000.

[53] These parameters were checked against independent measures of geomagnetic activity to verify that they are geophysically meaningful indicators of the Birkeland current system. The Net *dB*, *dBE**, and *dBW** were tested against quick look *AE*, *AU*, and *AL*. Reasonable agreement was found for the three example days corresponding to low to moderate, moderate, and high activity. The Net *dB* is correlated with quick look *AE* having a linear regression between log(Net *dB*) and log(*AE*) of 0.65 and 0.73 for Net *dB* derived from all MLT and nightside MLT, respectively. The equatorward extent of the region 1/region 2 sense perturbations (80% level) was correlated with *Kp*, regression coefficient of −0.68, consistent with expectations that the Birkeland current system expands equatorward with increasing geomagnetic activity. These comparisons with conventional ground magnetometer derived indices indicate

that the Iridium system measurements reflect the behavior of the same physical system that produces the ground perturbations.

[54] These tests were based on summary statistics of the magnetic perturbations and the distribution of perturbations above the data noise level. Spherical harmonic fitting analysis has also been applied to Iridium data to derive maps of magnetic perturbations and field-aligned current distributions [*Waters et al.*, 2001] and is invaluable for detailed quantitative estimation of the distribution and intensity of the FACs. The parameters introduced here complement the spherical harmonic analysis by providing a continuous key parameter data set that is more convenient to use both for survey purposes and for comparison with other time series data sets. The key parameters represent the most salient features of this globally distributed set of measurement points and provide information about the character of the data even when the perturbations levels are too low for more sophisticated analyses.

[55] Finally, the Iridium-derived parameters were evaluated for two geomagnetic storms, 22–23 September 1999 and 21–22 October 1999, and compared against the storm evolution as indicated by the provisional *Dst* and the IMF/solar wind observations from the ACE spacecraft. The Net *dB*, R12, and fraction of points above the noise level display pronounced correlation with IMF B_z indicating strong (weak) currents for southward (northward) B_z. Moreover, R12 expands equatorward (poleward) when B_z turns south (north). In addition, the northern and southern hemispheres independently display the same development of R12 and the latitude distribution of the fraction of points above the noise level. The storm results provide additional evidence that the Iridium system measurements provide a means to monitor the global Birkeland current system. More detailed behavior also appears to be present, including the expansion/contraction of R12 and dependence of the currents on IMF, in particular, the indications that the currents do not turn off for northward IMF provided B_y is still large. These results suggest that the Iridium data have the potential to yield important new clues about the solar wind-magnetosphere interaction.

[56] **Acknowledgments.** This work was supported by the National Space Weather Program under NSF grant ATM9819804. We are deeply indebted to the engineers and operations personnel of Motorola Inc. and Iridium Satellite LLC for providing the magnetic and satellite ephemeris data required for these analyses. We are grateful to the scientists and engineers of the Advanced Composition Explorer (ACE) spacecraft and to the Solar Wind Electron, Proton, and Alpha Monitor (SWEPAM) and the Magnetic Field Experiment (MAG) teams, whose data were also used for this work.

[57] Janet G. Luhmann thanks A. V. Koustov and another referee for their assistance in evaluating this paper.

References

Anderson, B. J., K. Takahashi, and B. A. Toth, Sensing global Birkeland currents with Iridium® engineering magnetometer data, *Geophys. Res. Lett.*, *27*, 4045–4048, 2000.

Armstrong, J. C., and A. J. Zmuda, Triaxial magnetic measurements of field-aligned currents at 800 km in the auroral region: Initial results, *J. Geophys. Res.*, *78*, 6802–6807, 1973.

Baker, K. B., and S. Wing, A new magnetic coordinate system for conjugate studies at high latitudes, *J. Geophys. Res.*, *94*, 9139–9143, 1989.

Cowley, S. W. H., Magnetosphere-ionosphere interactions: A tutorial review, in *Magnetospheric Current Systems*, *Geophys. Monogr. Ser.*, vol. 118, edited by S. Ohtani, pp. 91–106, Washington, D. C., 2000.

Cummings, W. D., and A. J. Dessler, Field-aligned currents in the magnetosphere, *J. Geophys. Res.*, *72*, 1007–1013, 1967.

Erlandson, R. E., L. J. Zanetti, T. A. Potemra, P. F. Bythrow, and R. Lundin, IMF B_Y dependence of region 1 Birkeland currents near noon, *J. Geophys. Res.*, *93*, 9804–9814, 1988.

Holzworth, R. H., and C.-I. Meng, Mathematical representation of the auroral oval, *Geophys. Res. Lett.*, *2*, 377–380, 1975.

Iijima, T., Field-aligned currents during northward IMF, in *Magnetospheric Currents*, *Geophys. Monogr. Ser.*, vol. 28, edited by edited by T. A. Potemra, pp. 115–122, AGU, Washington, D. C., 1984.

Iijima, T., Field-aligned currents in geospace: Substance and significance, in *Magnetospheric Current Systems*, *Geophys. Monogr. Ser.*, vol. 118, edited by S. Ohtani, pp. 107–129, Washington, D. C., 2000.

Iijima, T., and T. A. Potemra, The amplitude distribution of field-aligned currents at northern high latitudes observed by TRIAD, *J. Geophys. Res.*, *81*, 2165–2174, 1976a.

Iijima, T., and T. A. Potemra, Field-aligned currents in the dayside cusp observed by Triad, *J. Geophys. Res.*, *81*, 5971–5979, 1976b.

Iijima, T., R. Fujii, T. A. Potemra, and N. A. Saflekos, Field-aligned currents in the south polar cusp and their relationship to the interplanetary magnetic field, *J. Geophys. Res.*, *83*, 5595, 1978.

Iijima, T., T. A. Potemra, and L. J. Zanetti, Large-scale characteristics of magnetospheric equatorial currents, *J. Geophys. Res.*, *95*, 991–999, 1990.

Kamide, Y., A. D. Richmond, and S. Matsushita, Estimation of ionospheric electric fields, ionospheric currents, and field-aligned currents from ground magnetic records, *J. Geophys. Res.*, *86*, 801–813, 1981.

Lu, G., et al., High-latitude ionospheric electrodynamics as determined by the assimilative mapping of ionospheric electrodynamics procedure for the conjunctive SUNDAIL/ATLAS 1/GEM period of March 28–29, 1992, *J. Geophys. Res.*, *101*, 26,697–26,718, 1996.

Ohtani, S.-I., T. A. Potemra, P. T. Newell, L. J. Zanetti, T. Iijima, M. Watanabe, M. Yamauchi, R. D. Elphinstone, O. de la Beaujardiere, and L. G. Blomberg, Simultaneous prenoon and postnoon observations of three field-aligned current systems from Viking and DMSP-F7, *J. Geophys. Res.*, *100*, 119–136, 1995.

Press, W. H., B. P. Flannery, S. A. Teukolsky, W. T. Vetterling, *Numerical Recipes*, Cambridge Univ. Press, New York, 1987.

Richmond, A. D., and Y. Kamide, Mapping electrodynamic features of the high-latitude ionosphere from localized observations: Technique, *J. Geophys. Res.*, *93*, 5741–5759, 1988.

Sofko, G. J., R. Greenwald, and W. Bristow, Direct determination of large-scale magnetospheric field-aligned currents with SuperDARN, *Geophys. Res. Lett.*, *22*, 2041–2044, 1995.

Watanabe, M., T. Iijima, and F. J. Rich, Synthesis models of dayside field-aligned currents for strong interplanetary magnetic field B_y, *J. Geophys. Res.*, *101*, 13,303–13,319, 1996.

Waters, C. L., B. J. Anderson, and K. Liou, Estimation of global field aligned currents using Iridium magnetometer data, *Geophys. Res. Lett.*, *28*, 2165–2168, 2001.

Weimer, D. R., A new technique for the mapping of ionospheric field-aligned currents from satellite magnetometer data, in *Magnetospheric Current Systems*, *Geophys. Monogr. Ser.*, vol. 118, edited by S. Ohtani, pp. 381–388, Washington, D. C., 2000.

Zanetti, L. J., W. Baumjohann, and T. A. Potemra, Ionospheric and Birkeland current distributions inferred from the MAGSAT magnetometer data, *J. Geophys. Res.*, *88*, 4875–4884, 1983.

Zmuda, A. J., J. H. Martin, and F. T. Heuring, Transverse magnetic disturbances at 1100 km in the auroral region, *J. Geophys. Res.*, *71*, 5033–5045, 1966.

B. J. Anderson, K. Takahashi, and B. A. Toth, Johns Hopkins University Applied Physics Laboratory, 11100 Johns Hopkins Road, Laurel, MD 20723-6099, USA. (brian.anderson@jhuapl.edu)

T. Kamei, World Data Center, Kyoto University, Kyoto, Japan.

C. L. Waters, School of Mathematics and Physical Sciences, University of Newcastle, University Drive, Callaghan, New South Wales 2308, Australia. (physpuls8@cc.newcastle.edu.au)

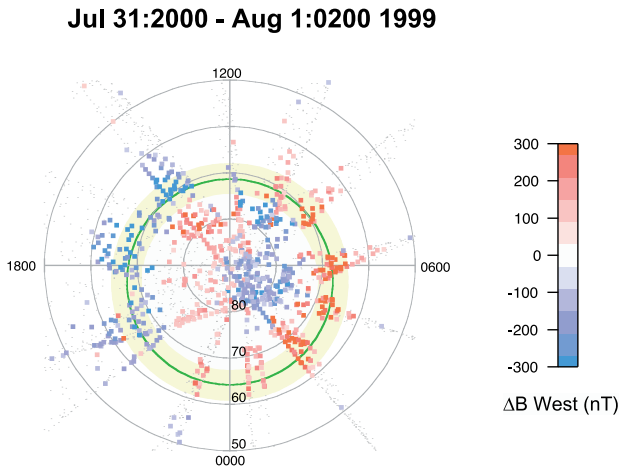

Figure 1. Polar view of Iridium system east-west magnetic perturbation data accumulated over a 6 hour period from 31 July to 1 August 1999. Data are plotted in Altitude-Adjusted Corrected Geomagnetic (AACGM) coordinates. Each magnetic reading is shown with gray, red, or blue dots, indicating measurements below threshold, westward above threshold, or eastward above threshold, respectively. The intensity of the colored dots reflects the magnitude of the perturbation. The green circle shows the least squares fit circle to the region 1/region 2 sense perturbations, and the yellow annulus indicates the range of radii that include 60% of the region 1/region 2 sense perturbations.